Coupling-Informed Data-Driven Scheme for Joint Angle and Frequency Estimation in Uniform Linear Array With Mutual Coupling Present

Yanming Zhang, *Member, IEEE*, Wenchao Xu, *Member, IEEE*, A-Long Jin, *Member, IEEE*, Min Li, *Member, IEEE*, Peifeng Ma, *Senior Member, IEEE*, Lijun Jiang, *Fellow, IEEE*, and Steven Gao, *Fellow, IEEE*

***Abstract*— This article proposes a novel coupling-informed data-driven algorithm tailored for the concurrent estimation of frequency and angle within a uniform linear array (ULA), while addressing the complicating influence of mutual coupling. Leveraging the hybrid dynamic mode decomposition (DMD) methodology, termed as averaged DMD, we incorporate moving average techniques to achieve effective denoising. The averaged DMD further decomposes the received signal into eigenvalues and corresponding eigenvectors. The frequency information is derived from the eigenvalues and the corresponding eigenvectors represent the steering vectors of sources. Subsequently, mutual coupling is informed into the calibration of the steering vector for each source. Specifically, the calibration of corresponding eigenvectors leverages the inverse of the mutual coupling matrix, i.e., Toeplitz matrix, acquired through Schur decomposition. Then, the calibrated steering vectors facilitate the estimation of angles. The decomposition results of our proposed method reveal a significant one-to-one correspondence between eigenvectors and eigenvalues, enabling automatic pairing of estimated frequencies and angles. Several numerical examples demonstrate the effectiveness and robust anti-noise properties of the proposed method, especially in scenarios where mutual coupling has a significant impact. Hence, our work contributes to the advancement of signal processing techniques in ULA applications, offering a promising avenue for enhanced performance in practical communication and radar systems.**

***Index Terms*— Automatic pairing, dynamic mode decomposition (DMD), joint angle and frequency estimation, moving average, mutual coupling, Schur decomposition.**

Received 23 March 2024; revised 6 September 2024; accepted 19 October 2024. Date of publication 30 October 2024; date of current version 19 December 2024. This work was supported in part by Chinese University of Hong Kong Start-up Fund under Grant 4937123, Grant 4937124, Grant 14223422, and Grant 14201923; in part by the Research Grants Council of Hong Kong under Grant GRF 14210623; in part by the General Program of the National Natural Science Foundation of China under Grant NSFC 62471332; in part by the Research Grants Council of the Hong Kong Special Administrative Region under Grant PolyU15225023; and in part by the Innovation and Technology Fund (ITF) under Grant ITP/007/23LP and Grant AoE/E-603/18.

Yanming Zhang and Steven Gao are with the Department of Electronic Engineering, The Chinese University of Hong Kong, Hong Kong, China (e-mail: ymzhang@eee.hku.hk; scgao@ee.cuhk.edu.hk).

Wenchao Xu is with the Department of Computing, The Hong Kong Polytechnic University, Hong Kong, China (e-mail: wenchao.xu@polyu.edu.hk).

A-Long Jin is with the Department of Communication and Networking, Xi'an Jiaotong-Liverpool University, Suzhou 215123, China (e-mail: along.jin@xjtlu.edu.cn).

Min Li is with the School of Microelectronics, Tianjin University, Tianjin 300072, China (e-mail: min_li@tju.edu.cn).

Peifeng Ma is with the Department of Geography and Resource Management, Institute of Space and Earth Information Science, The Chinese University of Hong Kong, Hong Kong (e-mail: mapeifeng@cuhk.edu.hk).

Lijun Jiang is with the Department of Communications and Networking, Missouri University of Science and Technology, Rolla, MO 65409 USA (e-mail: ljf82@mst.edu).

Color versions of one or more figures in this article are available at https://doi.org/10.1109/TAP.2024.3485251.

Digital Object Identifier 10.1109/TAP.2024.3485251

I. Introduction

DIRECTION of arrival (DOA) estimation plays a pivotal role in array signal processing applications [1], [2], [3], such as radar [4], [5], sonar [6], [7], and wireless communications [8], [9]. Precise knowledge of the angles from which signals arrive is crucial for beamforming [10], [11], source localization [12], [13], [14], and communication system performance [15], [16], [17]. However, real-world scenarios introduce challenges for DOA estimation, such as position error, gain-phase error, and mutual coupling, with mutual coupling emerging as a prominent concern in antenna array configurations [15], [18], [19], [20]. Herein, mutual coupling refers to undesired interaction among antenna elements, complicating the accurate estimation of DOA [21]. In particular, the presence of mutual coupling within antenna arrays can give rise to a model mismatch in the process of estimating the DOA [15]. This model mismatch, stemming from the interantenna interactions induced by mutual coupling, has the potential to significantly compromise the accuracy and reliability of DOA estimation, resulting in a notable degradation in the overall performance of the estimation process [18], [19], [20].

To address this issue, various methods have been proposed to mitigate the mutual coupling side effect. Specifically, electromagnetic models are used to describe the mutual coupling effects in antenna arrays, such as method of moments (MoM) [22], [23] and finite element method (FEM) [24], which involve numerical solutions to evaluate the interactions between antennas. However, this calculation necessitates preexisting knowledge of the incoming signals, which adds an additional layer of complexity to the DOA estimation process. Another kind of approach is to use the mutual coupling calibration methods. For instance, Ng and See [25] proposed the maximum-likelihood (ML)-based method for DOA estimation via calibration sources. Sellone and Serra [26] developed an online mutual coupling calibration algorithm

with an iterative procedure for the angle finding of uniform linear array (ULA). Liao et al. [18] proposed three modified subspace approaches for tracking the mutual coupling effect by carefully designing based on covariance calibration of matrix of the entire observations. There are also several other mutual coupling calibration methods, but due to space limitations, they will not be presented herein. Recently, with the rapid advancement of artificial intelligence, an increasing array of machine learning and data-driven methods has provided fresh insights into addressing this classical problem. Several neural-network-based approaches have been developed for DOA estimation with mutual coupling present, such as artificial neural network (ANN) [27], convolutional neural network (CNN) [28], [29], and generative adversarial network (GAN) [30], [31]. However, these methods require labeled data for training, which can be prohibitive, and often lack broad generalizability. Moreover, noise constitutes a significant interference in DOA estimation [32]. Effectively achieving DOA estimation with mutual coupling present in high-noise environments poses a challenge and remains a subject of ongoing research and development [33]. The existing methodologies address mutual coupling to varying extents, yet achieving simultaneous DOA and frequency estimation under these conditions, alongside automatic matching and robust noise resistance, remains an unresolved research gap.

In this article, we present a novel coupling-informed data-driven approach, i.e., Schur-averaged dynamic mode decompositions (DMD), designed for simultaneous DOA and frequency estimation using a ULA in scenarios characterized by mutual coupling and high noise levels. By integrating the moving average technique within the DMD framework, referred to as averaged DMD, anti-noise capabilities are enhanced. The proposed averaged DMD method directly decomposes the observed data into DMD eigenvalues and eigenvectors, where the eigenvalues convey frequency information. The eigenvectors undergo calibration through the Schur decomposition of the mutual coupling matrix. Subsequently, DOA estimation for each source is derived based on the calibration of individual eigenvectors. Ultimately, concurrent frequency and DOA estimations are achieved. Our contributions are succinctly summarized as follows.

1) We establish a novel coupling-informed data-driven scheme, namely, Schur-averaged DMDs, for the joint DOA and frequency estimation in ULA with mutual coupling present. The significance of this novel scheme lies in integrating coupling information into the data-driven framework, acknowledging, and leveraging the influence of mutual coupling in the estimation process. This incorporation aims to enhance the accuracy and robustness of joint DOA and frequency estimation in realistic scenarios.
2) The integration of the moving averaging technology into the DMD framework stands as a pivotal enhancement, specifically devised to fortify the anti-noise capabilities of the proposed data-driven method. This incorporation is designed to augment the robustness of the DMD-based approach in the presence of noise, thereby contributing to an improved and more reliable frequency estimation performance. The adaptive nature of the moving averaging technology within the DMD framework allows for effective noise mitigation, ensuring a more accurate decomposition of underlying signal component and, consequently, a heightened resistance to adverse noise effects during the estimation process.
3) The inherent one-to-one correspondence between eigenvalues and eigenvectors within the DMD framework benefits automatic pairing in the estimations. This inherent characteristic streamlines the joint estimation process by directly associating the estimated frequency and DOA without necessitating supplementary matching steps. The seamless relationship between eigenvalues and eigenvectors contributes to the method's efficiency, offering a straightforward and automated means of pairing essential parameters, thereby enhancing the simplicity and accuracy of the overall estimation procedure.
4) The proposed method can adapt to scenarios where the number of sources is unknown. This adaptability is based on the analysis of the distribution of eigenvalues, allowing for the determination of the actual number of the source during the estimation process. This feature enhances the versatility and practical applicability of the proposed method in real-world scenarios where source counts may be ambiguous or *prior* unknown.

The remainder of the article are outlined as follows. Section II provides the mathematical formulations governing the research problem of interest. Section III delineates the proposed methodology, elucidating the details of the Schur-averaged DMD approach. Then, Section IV provides several numerical examples to validate the proposed method. The conclusion to this study is presented in Section V.

II. Formulation

A. Signal Model in ULA

Without loss of generality, an antenna array comprising M omnidirectional antennas is considered, where the center frequency of interest is denoted as f_c. Assume the existence of I uncorrelated narrowband sources $\{r_i(t)\}$ impinging on the array, each exhibiting frequencies centered at $f_c + f_i$, with $i = 1, \ldots, I$. Herein, f_c means the carrier's frequency, and f_i refers to the baseband of the ith source. After downconversion to baseband, i.e., f_i, the observed signal at the ith antenna element, represented as $y_i(t)$, can be expressed as a summation over M sources, which is expressed as follows [34], [35]:

$$y_i(t) = \sum_{i=1}^{I} a_m(\theta_i) r_i(t) e^{j2\pi f_i t} + n_m(t), \quad m = 1, \ldots, M \tag{1}$$

where $a_m = e^{-j2\pi\phi_m(\theta_i)}$ represents the antenna response to the ray from direction θ_i, where $\phi_m(\theta_i)$ is influenced by the geometric pattern of the antennas. For instance, in a ULA, $\phi_m(\theta_i) = f_c d(m-1)\sin\theta_i/c$, where c is the wave propagation speed, and d is the antenna spacing. The additive noise term $n_m(t)$ adheres to spatial and temporal white Gaussian characteristics with zero mean and variances σ_n^2. In the case of

narrowband signals in a slow-fading environment, the signals are block fading, implying that $r_i(t)$ remains constant within a short period of the signal samples. Often, the number of the sources (I) is assumed to be known or has been estimated via minimum description length principle or Akaike information criterion [36].

Upon appending N time samples at the I receive antennas, the kth block signal is formulated as [37]

$$\mathbf{Y}(k) = \mathbf{A}\mathbf{S}(k)\mathbf{G}^H + \mathbf{N}(k). \tag{2}$$

Here, $\mathbf{Y}(k) = [\mathbf{y}(t_k), \mathbf{y}(t_k + \Delta t), \ldots, \mathbf{y}(t_k + (K-1)\Delta t)]$, with t_k being the sampling reference time of the kth block, Δt refers to the sampling period, $\mathbf{y}(t_k) = [y_1(t_k), \ldots, x_M(t_m)]^T$, and $\mathbf{Y}(k) \in \mathbb{C}^{M\times K}$. $\mathbf{A} = [\mathbf{a}(\theta_1), \ldots, \mathbf{a}(\theta_I)]$ denotes the $M \times I$ spatial steering matrix with the spatial steering vector $\mathbf{a}(\theta) = [e^{-j2\pi\phi_1(\theta)}, e^{-j2\pi\phi_2(\theta)}, \ldots, e^{-j2\pi\phi_M(\theta)}]^T$. $\mathbf{S}(k) = \text{diag}\{\mathbf{s}(t_k)\}$ refers to the signal matrix, whose diagonal elements are $\mathbf{s}(t_k) = [s_1(t_k), \ldots, s_I(t_k)]^T$. $\mathbf{G} = [\mathbf{g}(f_1), \ldots, \mathbf{g}(f_I)]$ denotes the $K \times I$ temporal signature matrix, in which the temporal signature vector $\mathbf{g}(f_i) = [1, e^{j2\pi f_i/f_s}, \ldots, e^{j2\pi f_i(K-1)/f_s}]^T$ with f_s denoting the sampling rate. $\mathbf{N}(k) = [\mathbf{n}(t_k), \mathbf{n}(t_k + \Delta t), \ldots, \mathbf{n}(t_k + (K-1)\Delta t)]$ means the noise matrix, whose column is $\mathbf{n}(t_k) = [n_1(t_k), \ldots, n_M(t_k)]^T$.

B. Signal Model in ULA With Mutual Coupling Present

In case of ULA with M antenna, the mutual coupling effect can be generally expressed as [38] and [39]

$$\mathbf{C} = \begin{bmatrix} C_{1,1} & C_{1,2} & \cdots & C_{1,N} \\ C_{2,1} & C_{2,2} & \cdots & C_{2,N} \\ \vdots & \vdots & \ddots & \vdots \\ C_{N,1} & C_{N,2} & \cdots & C_{N,N} \end{bmatrix} \tag{3}$$

where $C_{i,j}$ represents the mutual coupling coefficient between the ith and jth sensors of the ULA. Since the coupling interaction between the ith and jth sensors is consistent, the mutual coupling effect can be expressed as a symmetric Toeplitz matrix as follows [40]:

$$\boldsymbol{C} = \text{Toeplitz}\{1, c_1, \ldots, c_m, \ldots, c_{M-1}\}. \tag{4}$$

Often, the mutual coupling between two sensors is inversely related to their distance, and thus it can be ignored when these two sensors are separated by few wavelengths. Therefore, for a ULA with M sensor elements, the MCM can be sufficiently modeled as a banded symmetric Toeplitz matrix as follows [41]:

$$\boldsymbol{C} = \text{Toeplitz}\left\{1, c_1, \ldots, c_{D-1}, \mathbf{0}^{1\times(M-D)}\right\}. \tag{5}$$

Clearly, when the distance between two sensors is more than D intersensor spacing, the mutual coupling coefficients are assumed to be zero.

Thus, following (2), the receiving signal via the ULA with the mutual coupling present can be expressed as [40]

$$\mathbf{X}(k) = \mathbf{C}\mathbf{A}\mathbf{S}(k)\mathbf{G}^H + \mathbf{N}(k) \tag{6}$$

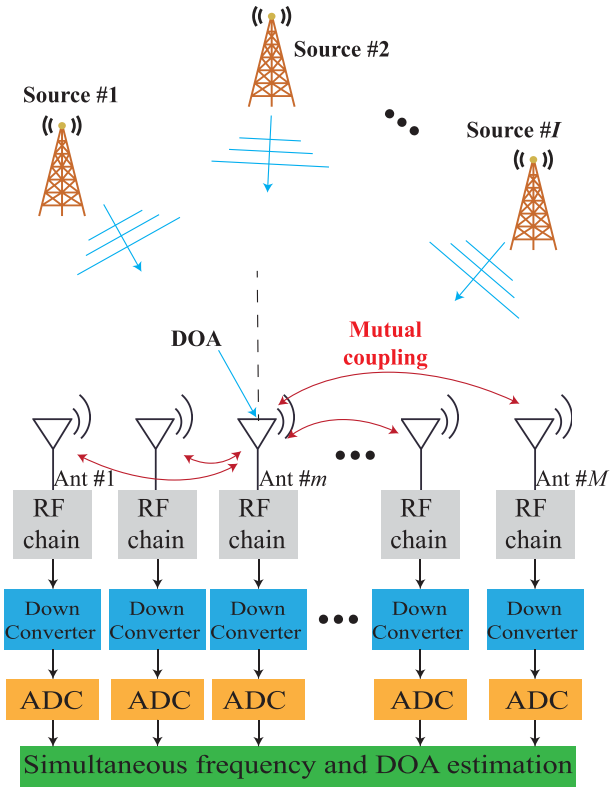

Fig. 1. Illustration of the simultaneous frequency and DOA estimation via the ULA with the mutual coupling present.

where $\mathbf{X}(k) \in \mathbb{C}^{M\times K}$. Correspondingly, taking the mutual coupling into account, the true steering vector should be rewritten as

$$\mathbf{a}_{\text{MC}}(\theta_i) = \mathbf{C}\mathbf{a}(\theta_i). \tag{7}$$

Fig. 1 illustrates the envisaged scenario of interest, incorporating the presence of mutual coupling. In the following, we present that our proposed method can extract the true steering vector at each frequency and obtain the actual DOA by introducing coupling information.

III. Proposed Coupling-Informed Data-Driven Scheme

A. Frequency Estimation via DMD

DMD, as a purely data-driven method, has been applied in various fields, such as hydrodynamics [42], [43], orbital angular momentum demultiplexing [44], [45], sea clutter [46], and electromagnetic radiation prediction [47]. Herein, the DMD is applied for the analysis of direct data from the ULA. Specifically, following the signal model in ULA with mutual coupling present as shown in (6), the observed data at the kth block can be represented as

$$\mathbf{X}(k) = [\mathbf{x}(t_k), \mathbf{x}(t_k + \Delta t), \ldots, \mathbf{x}(t_k + (K-1)\Delta t)]. \tag{8}$$

First, the DMD sorts this observed data matrix, i.e., $\mathbf{X}(k)$, into two adjacent matrixes, which are given as [47]

$$\mathbf{X}_1 = [\mathbf{x}(t_k), \mathbf{x}(t_k + \Delta t), \ldots, \mathbf{x}(t_k + (K-2)\Delta t)] \tag{9}$$

$$\mathbf{X}_2 = [\mathbf{x}(t_k + \Delta t), \mathbf{x}(t_k + 2\Delta t), \ldots, \mathbf{x}(t_k + (K-1)\Delta t)]. \tag{10}$$

Based on linear mapping assumption, the relationship between (9) and (10) can be linked by a mapping matrix as

$$\mathbf{X}_2 = \mathbf{B}\mathbf{X}_1. \tag{11}$$

Then, the DMD is to compute the eigenvalue and the corresponding eigenvector of mapping matrix $\mathbf{B}$. Herein, the singular value decomposition (SVD)-based method is applied for the calculation. The details can be found in Appendix. Finally, DMD models the direct data from ULA with mutual coupling present as

$$\mathbf{x}(t) = \sum_{i=1}^{I} p_i \mathbf{h}_i e^{\omega_i t} = \sum_{i=1}^{I} p_i \mathbf{h}_i e^{\omega_i^r t} e^{j\omega_i^i t}. \tag{12}$$

Herein, $\mathbf{h}_i$ refers to the ith column of the matrix $\mathbf{H}$, $\omega_i = \omega_i^r + j\omega_i^i = \ln(\lambda_k)/\Delta t$, and p_i means the amplitude weight of the ith dynamic mode.

Finally, comparing (12) with (1), we can see that the superposed incoming ray signals are decomposed into I modes. ω_i implies the frequency information of the ith incoming ray, which can be estimated by

$$\hat{f}_i = \frac{\omega_i}{2\pi} \tag{13}$$

where $\hat{(\cdot)}$ denotes the estimated values. Hence, the frequency information can be obtained from the decomposed ω_i. Notably, $p_i \boldsymbol{h}_i$ implies the corresponding spatial distribution of the ith incoming ray.

When the a *prior* knowledge of the source number I is available, SVD step in DMD is executed with truncation at I [refer to (27)]. In this specific case, the eigendecomposition of the mapping matrix in the low-dimensional system directly yields the eigenvalues and eigenvectors corresponding to the actual signal sources. However, in practical scenarios, the true number of signals is often unknown beforehand, introducing a new parameter requiring estimation. To tackle this challenge, a threshold is introduced for truncating the SVD, where the threshold exceeds the presumed number of signals. Consequently, this approach yields more eigenvalues in the DMD eigenvalues' distribution than the number of signals. The determination of the actual number of signals is then contingent upon assessing whether the real part of the eigenvalues is zero. Formally, the estimated source number $\hat{I}$ is defined as

$$\hat{I} = \sum_{i=1}^{N} \mathbb{1}(\text{real}(\omega_i) < \varepsilon_0). \tag{14}$$

Here, $\hat{I}$ signifies the estimated number of sources, N refers to the truncation order in the SVD operation, and ε_0 represents the error threshold, a small predetermined value. It is imperative to note that the truncation order of the SVD N should exceed the actual number of signal sources, ensuring accurate estimation $N > I$. In practice, setting I to a sufficiently large value guarantees the correct estimation of the source count. In the following, we introduce that the DOA can be estimated based on this corresponding spatial distribution after the coupling-informed calibration.

B. Moving Average of Adjacent Snapshot Sequences

Incorporating the moving average approach into DMD proves effective in mitigating the impact of disruptive noise on the computation of the mapping matrix. The core of the DMD-based method involves determining the principal eigenvalues and eigenvectors of the mapping matrix denoted as $\mathbf{B}$ in $\mathbf{X}_2 = \mathbf{B}\mathbf{X}_1$ [refer to (11)]. This computation relies on the assumption that two consecutive columns, labeled as $\mathbf{x}(t_k + k\Delta t)$ and $\mathbf{x}(t_k + (k+1)\Delta t)$, are linked through a linear mapping function $\mathbf{F}$. Specifically, $\mathbf{x}(t_k + (k+1)\Delta t) = \mathbf{F}\mathbf{x}(t_k + k\Delta t)$.

To minimize noise impact on the mapping matrix, the moving average approach is used. Specifically, the adjacent η columns are summed and averaged, expressed as follows:

$$\sum_{k=1}^{\eta} \overline{\overline{\mathbf{x}}}(t_k + k\Delta t) = \sum_{k=1}^{\eta} \overline{\overline{\mathbf{x}}}^{s}(t_k + k\Delta t) + \sum_{k=1}^{\eta} \overline{\overline{\mathbf{x}}}^{n}(t_k + k\Delta t) \tag{15}$$

where $\overline{\overline{(\cdot)}}$ denotes states in the moving average process, $\overline{\overline{\mathbf{x}}}^{s}(t_k + k\Delta t)$ signifies the signal component, and $\overline{\overline{\mathbf{x}}}^{n}(t_k + k\Delta t)$ represents the noise component. Notably, controlling η is crucial to ensuring that data from the 1st to ηth points are spaced less than $1/4$ of the period. Moreover, this approach maintains signal space integrity by effectively attenuating the noise component, given the zero mean of Gaussian noise

$$\overline{\overline{\mathbf{X}}}_2 = \overline{\overline{\mathbf{B}}}\ \overline{\overline{\mathbf{X}}}_1. \tag{16}$$

Clearly, states in the moving average process remain related through the mapping matrix. Through DMD calculation, the eigenvalues and eigenvectors, with noise suppressed, can be determined.

C. Coupling-Informed Calibration of the Steering Vector

In the following, we analyze the spatial distribution obtained from the decomposition, i.e., the product of dynamic modes and amplitudes ($p_i \boldsymbol{h}_i$), for which we can estimate the DOA associated with the ith incoming ray. Initially, we address decoupling using the spatial distribution of the ith incoming ray.

First, we use the known mutual coupling matrix, which is Toeplitz, and apply Schur decomposition to find its inverse. In particular, given the information that a Toeplitz matrix $\mathbf{C}$ is used for the mutual coupling effect in ULA, it can be decomposed into the product of two matrices $\mathbf{Q}$ and $\mathbf{R}$, which can be represented as [48] and [49]

$$\mathbf{C} = \mathbf{Q}\mathbf{R} \tag{17}$$

where $\mathbf{Q}$ is the unitary matrix and matrix $\mathbf{R}$ is the upper triangular matrix. To calculate the inverse of $\mathbf{C}$, one can use

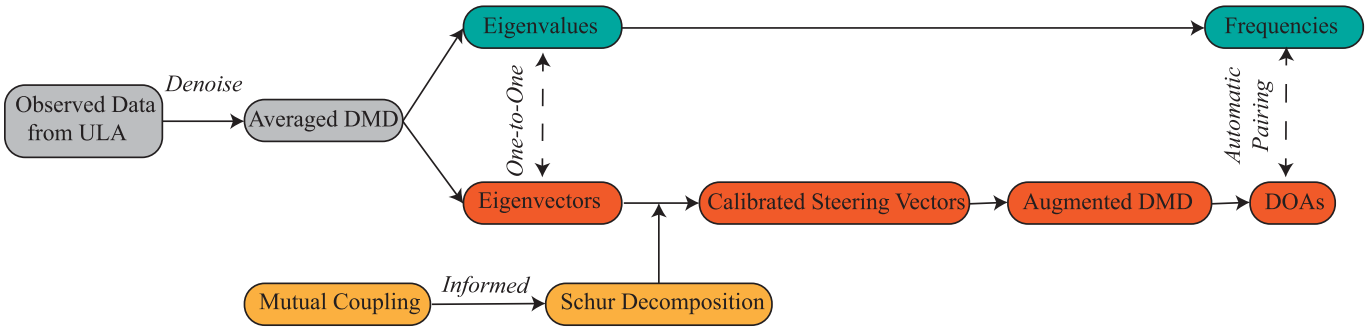

Fig. 2. Flowchart of the proposed coupling-informed data-driven method for joint angle and frequency estimation in the ULA with mutual coupling present.

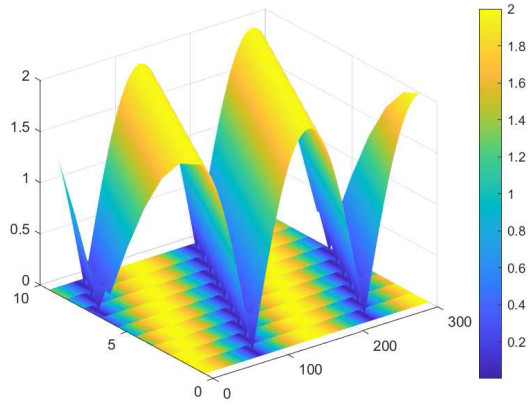

(a)

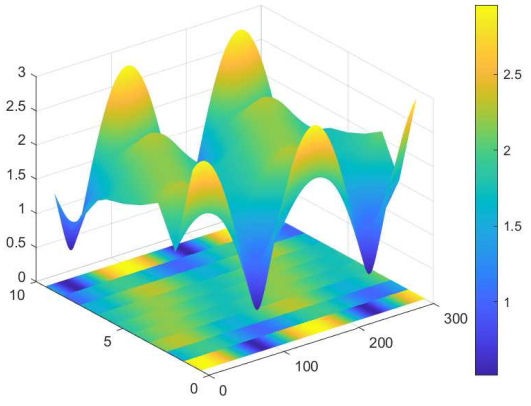

(b)

Fig. 3. Amplitude distribution. (a) Original distribution. (b) Mutual coupling distribution.

the following relation:

$$\mathbf{C}^{-1} = \mathbf{R}^{-1}\mathbf{Q}^{*}. \tag{18}$$

Herein, $\mathbf{Q}^{*}$ denotes the conjugate transpose of $\mathbf{Q}$. Then, we use this decomposition of the inverse of $\mathbf{C}$ for the calibration of the steering vector, which can be expressed as follows:

$$\mathbf{a}_{\mathrm{DSV}}(\theta_i) = \mathbf{C}^{-1} p_i \boldsymbol{h}_i = \mathbf{R}^{-1}\mathbf{Q}^{*} p_i \boldsymbol{h}_i \tag{19}$$

where $\mathbf{a}_{\mathrm{DSV}}(\theta_i)$ refers to as the decoupled steering vector. Compared with (7), mutual coupling effects are eliminated

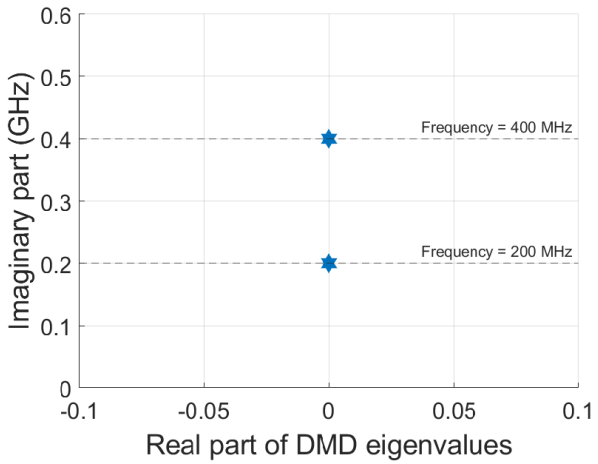

Fig. 4. Comparison between the decomposed eigenvalues of augmented DMD and the actual frequency in Fig. 3(b).

in each individual spatial distribution. That is to say, the decoupled steering vector, i.e., $\mathbf{a}_{\mathrm{DSV}}(\theta_i)$, should theoretically be the same as the array steering vector without coupling, i.e., $\mathbf{a}(\theta_i)$. Thus, we obtain the calibrated spatial distribution.

Then, the DOA is derived based on the calibrated spatial distribution. Similarly, we use the ith calibrated spatial distribution, i.e., $\mathbf{a}_{\mathrm{DSV}}(\theta_i)$, as an example. Its elements can be expressed as

$$\mathbf{a}_{\mathrm{DSV}}(\theta_i)^{T} = \left[a_1^i, a_2^i, \ldots, a_m^i, \ldots, a_M^i\right] \tag{20}$$

where the superscript indicates the index of the calibrated spatial distribution, and the subscript indicates the index of the antenna in the array. Then augmented DMD is used to model this 1-D vector. Specifically, the original calibrated spatial distribution is reshaped into the corresponding Hankel matrix $\mathbf{E}$ which is constructed as follows:

$$\mathbf{E} = \begin{bmatrix} a_1^i & a_2^i & \cdots & a_{M-e+1}^i \\ a_2^i & a_3^i & \cdots & a_{M-e+2}^i \\ \vdots & \vdots & \ddots & \vdots \\ a_e^i & a_{e+1}^i & \cdots & a_M^i \end{bmatrix} \tag{21}$$

where e refers to the index delay of ULA. Then, the DMD is performed based on the constructed Hankel matrix $\mathbf{E}$. Similarly, then, $\mathbf{E}$ is split into $\mathbf{E}_1$ and $\mathbf{E}_2$, which are given

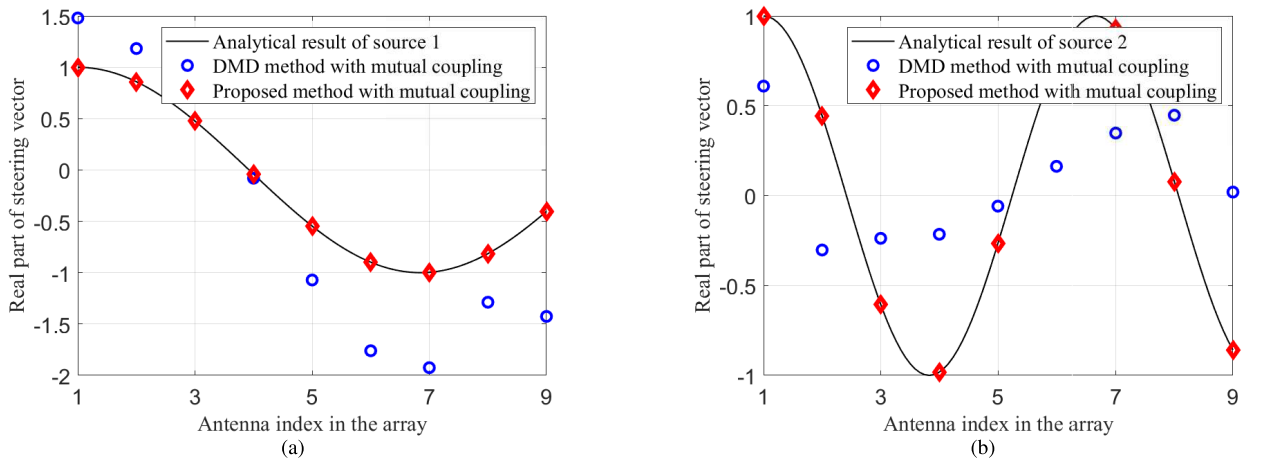

Fig. 5. Results of the steering vector. (a) First source. (b) Second source.

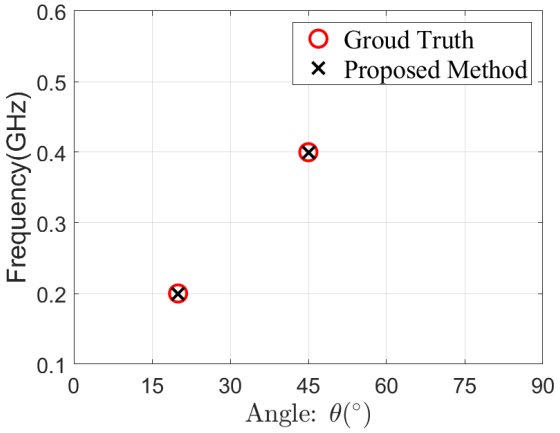

Fig. 6. Joint results of DOA and frequency via ULA with two incoming raying (sources).

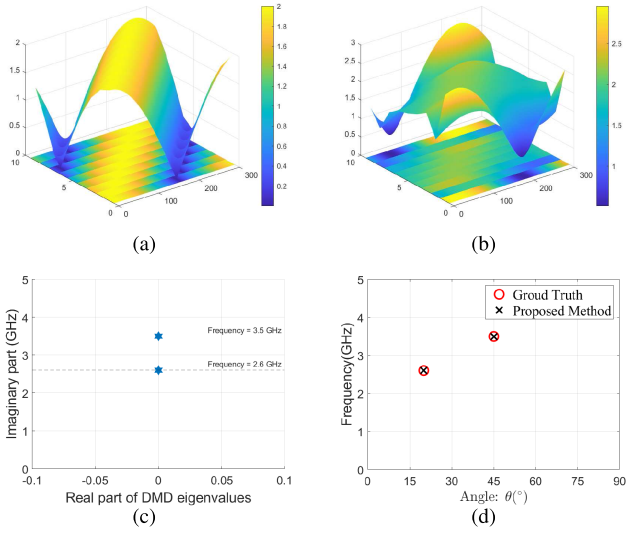

Fig. 7. Analysis result at 2.6 and 3.5 GHz. (a) Original amplitude distribution, (b) mutual coupling amplitude distribution, (c) comparison between the decomposed eigenvalues of augmented DMD and the actual frequency, and (d) joint results of DOA and frequency via ULA with two sources.

as

$$\mathbf{E}_1 = \begin{bmatrix} a_1^i & a_2^i & \cdots & a_{M-e}^i \\ a_2^i & a_3^i & \cdots & a_{M-e+1}^i \\ \vdots & \vdots & \ddots & \vdots \\ a_e^i & a_{e+1}^i & \cdots & a_{M-1}^i \end{bmatrix} \tag{22}$$

$$\mathbf{E}_2 = \begin{bmatrix} a_2^i & a_3^i & \cdots & a_{M-e+1}^i \\ a_3^i & a_4^i & \cdots & a_{M-e+2}^i \\ \vdots & \ddots & \vdots & \\ a_{e+1}^i & a_{e+2}^i & \cdots & a_M^i \end{bmatrix}. \tag{23}$$

Next, due to the linear mapping assumption, the relationship between (22) and (23) can be written as

$$\mathbf{E}_2 = \mathbf{O}\mathbf{E}_1. \tag{24}$$

Similarly, based on the computation of eigenvalues and eigenvectors of $\mathbf{O}$, the delay state $\mathbf{a}^i$ can be modeled as

$$\mathbf{a}^i = \sum_{q=1}^{Q} l_q \mathbf{z}_q e^{\xi_q m} = \sum_{q=1}^{Q} l_q \mathbf{z}_q e^{\xi_p^r m} e^{j\xi_p^i m} \tag{25}$$

where l_q, $\mathbf{z}_q$, and ξ_q, respectively, mean the qth amplitude, delay dynamic mode, and eigenvalues. Since each calibrated spatial distribution solely corresponds to one incoming ray. Hence, the rank of the eigendecomposition of $\mathbf{O}$ should be equal to one, such that $Q = 1$. In addition, m denotes the index of the antennas in the ULA.

Finally, comparing ξ_q with $\phi_m(\theta_i) = f_c d(m-1)\sin\theta_i/c$, the DOA can be obtained by

$$\hat{\theta}_i = \arcsin\left(\frac{\xi_p^i c}{2\pi f_c d}\right). \tag{26}$$

Clearly, the DOA of the ith incoming ray is estimated. For each spatial distribution, we conduct this augmented DMD analysis, yielding the DOA for each incoming ray.

D. Automatic Pairing of Estimated Angle and Frequency

Due to the inherent one-to-one correspondence between eigenvalues, i.e., ω_i and eigenvectors, i.e., $p_i\mathbf{h}_i$ in the DMD framework [see (12)], a noteworthy observation emerges.

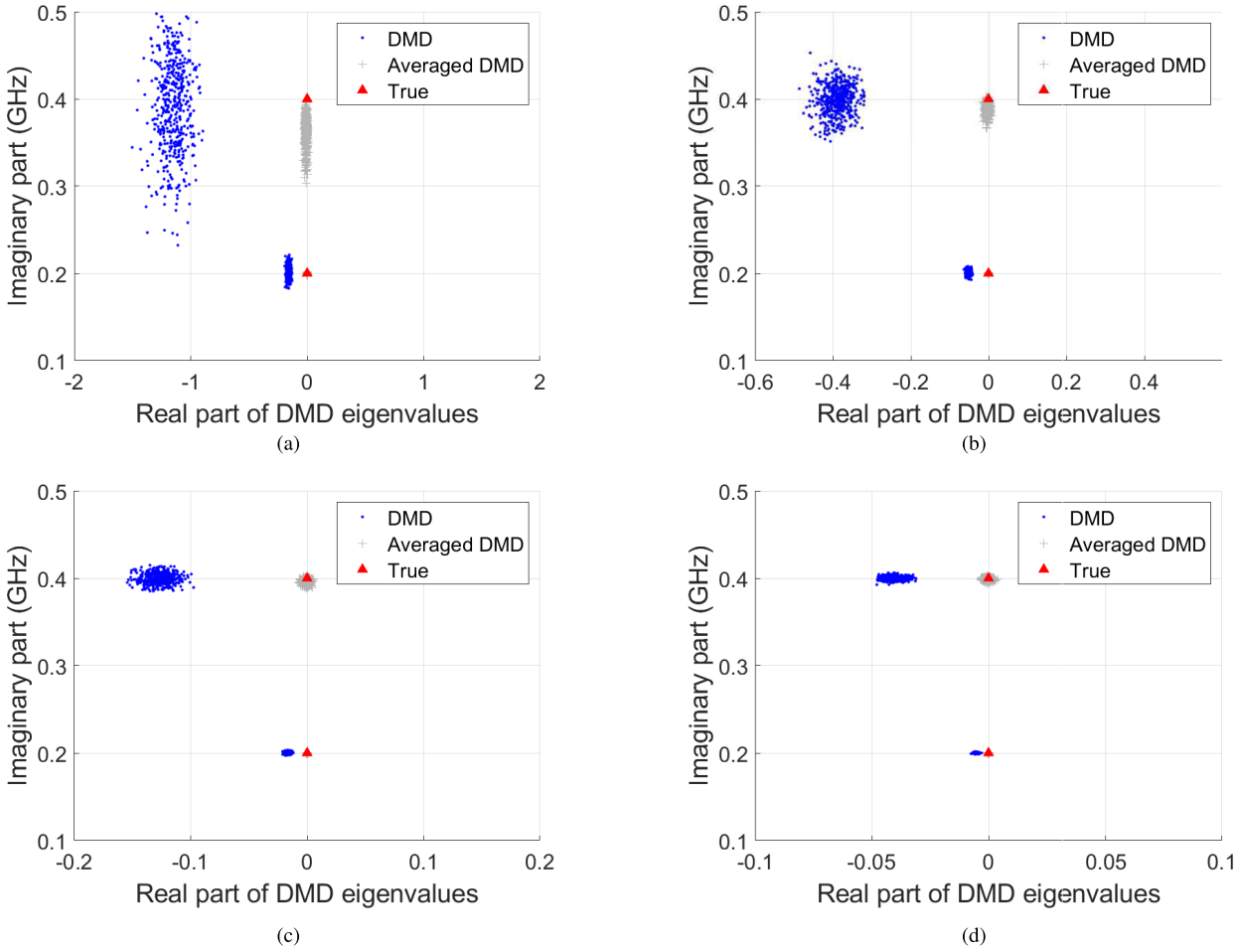

Fig. 8. Comparison results of DMD and averaged DMD of 500 Monte Carlo runs under different SNRs. (a) 0 dB, (b) 5 dB, (c) 10 dB, and (d) 15 dB.

Specifically, as the frequencies of each incoming ray are derived from the eigenvalues, the associated eigenvectors serve a pivotal role in the subsequent analysis for estimating the DOA. This unique characteristic establishes an unambiguous relationship between the obtained frequencies and their corresponding DOAs. As a result, upon deriving the outcomes, the necessity for an auxiliary matching algorithm to align the estimated frequencies with the DOAs becomes superfluous. In essence, this methodology seamlessly integrates an automatic matching capability into the estimation process, contributing to the efficiency and reliability of the estimation analysis within the DMD framework. Notably, as long as the sampling frequency is within an appropriate range, our proposed approach can be effectively used for joint DOA and frequency estimation across various frequencies. Fig. 2 shows plots of the flowchart of the proposed coupling-informed data-driven method. Notably, our method is specifically applicable to scenarios involving mutual coupling with the Toeplitz matrix assumption.

IV. Results

A. Joint Estimation for Two Sources

In the following, we conduct a comprehensive validation of our proposed methodology using a ULA composed of nine antennas. The primary objective is to assess the effectiveness of our approach in mitigating the impact of mutual coupling in antenna arrays. The mutual coupling is described as the following matrix: $\boldsymbol{C} = \text{Toeplitz}\{1, 0.75e^{-j(\pi/3)}, 0.45e^{j(pi/3)}, 0.15e^{j(pi/10)}, \mathbf{0}^{1\times 5}\}$. To commence, Fig. 3 visualizes the amplitude of the field distribution of the ULA with and without the mutual coupling, which serves as the baseline for subsequent assessments. Comparing Fig. 3(a), depicting the scenario without mutual coupling, to Fig. 3(b), where spatial distribution is influenced by mutual coupling, reveals notable changes. In the presence of mutual coupling, the spatial distribution undergoes alterations, manifesting as a decrease in reception amplitudes for certain antennas and an increase for others. In other words, the energy received becomes unevenly distributed across the antennas due to the presence of coupling. This underscores the necessity for calibration methods to achieve the desired accuracy under such mutual coupling conditions.

Through the augmented DMD, the measured field data with mutual coupling are decomposed into the dynamic modes and the associated eigenvalues. These obtained eigenvalues are crucial indicators of the source's frequency information [see (13)]. We compare these eigenvalues against the ground truth, providing a quantitative measure of the accuracy of the

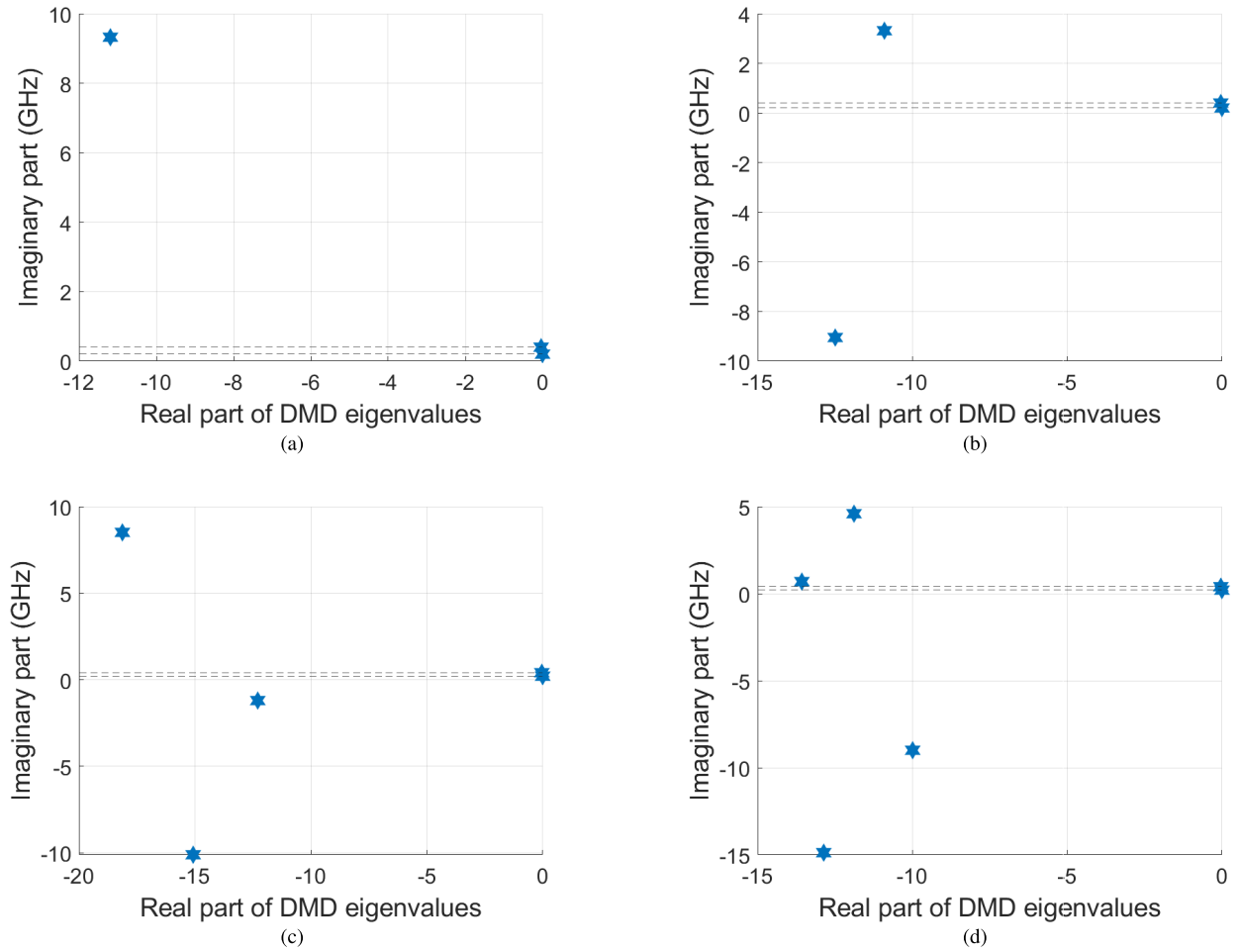

Fig. 9. Visualization of DMD eigenvalues' distribution with truncation orders. (a) 3, (b) 4, (c) 5, and (d) 6 in scenarios where the number of sources is unknown.

augmented DMD-based analysis. Based on (13), the comparison between the eigenvalues of augmented DMD and the real frequency is shown in Fig. 4. It is clear that the estimated frequencies, i.e., 200 and 400 MHz, consist of the actual ones. Hence, we can conclude that the extracted eigenvalues can imply the frequency information. Notably, the corresponding eigenvectors can be used for the estimation of the DOA. In the following, we detail the estimation of DOA according to the calibration of the steering vector based on these extracted eigenvectors.

Due to the mutual coupling present, the calibration of the steering vectors is needed. In this content, the eigenvectors decomposed by the augmented DMD corresponds to the steering vector of each source. Leveraging Schur decomposition for inversion, we realize the calibration of the each decomposed eigenvector. Fig. 5(a) and (b) shows the side-by-side comparison between the obtained eigenvector, calibrated eigenvector, and the ground truth. The close agreement between the calibrated eigenvector and the actual ones validates the efficacy of our calibration approach. We emphasize the significance of this step in refining the accuracy of the estimation of DOA, particularly in the presence of mutual coupling. Based on this calibration, the DOA can be computed. Notably, each eigenvalue solely corresponds to one source, and each eigenvalue solely corresponds to the eigenvector. So each eigenvector implies one DOA information. Then, the DOA information is obtained also corresponding to the frequency information. Thus, the estimated DOA and frequency are automatic paired. Fig. 6 shows the joint estimation results. It can be seen that the estimated DOA and frequency agree well with the actual one. Hence, we can conclude that the proposed method can estimate the DOA and frequency with automatic pairing under the mutual coupling conditions.

To further verification, we consider an example with 2.6 and 3.5 GHz, of which frequency bands are commonly used in 5G networks. The other parameters, including DOA and mutual coupling, are the same as those shown in Fig. 3. Fig. 7(a) shows the original amplitude distribution, and Fig. 7(b) shows plots of the mutual coupling amplitude distribution. Through the proposed method, the decomposed eigenvalues of augmented DMD are obtained, which are shown in Fig. 7(c). For the comparison, the actual frequency is also plotted. It is clear that the eigenvalues of augmented DMD imply the correct frequency information, namely, 2.6 and 3.5 GHz. Besides, Fig. 7(d) shows plots of the joint results of DOA and frequency via ULA with two sources. It can be seen that the DOA and

frequency are obtained and paired correctly. Therefore, we can conclude that the proposed method can be used to jointly estimate DOA and frequency with mutual coupling, and the frequency range in which the proposed method is applicable is arbitrary.

B. Denoising Performance of Averaged DMD

In the ensuing analysis, we use the example of two sources, as shown in Fig. 3, to substantiate the efficacy of denoising through the application of the averaged DMD. Specifically, we undertake a comparison of the denoising performance exhibited by the traditional DMD and its averaged counterpart across 500 Monte Carlo runs, varying the signal-to-noise ratio (SNR). The outcomes of this comparative assessment are plotted in Fig. 8(a)–(d), corresponding to distinct SNR conditions of 0, 5, 10, and 15 dB, respectively.

From the discernment of Fig. 8, it is evident that the denoising outcomes achieved through averaged DMD surpass those attained by DMD across all the considered SNR conditions. This signifies that the results produced by averaged DMD closely align with the actual values. Notably, as the SNR diminishes, the performance of DMD exhibits a progressive deterioration, whereas the error incurred by averaged DMD remains within acceptable bounds. In addition, in the comparative evaluation of two distinct frequencies, it is observed that the absolute error associated with a higher frequency surpasses that of a lower frequency, which is an observation consistent in both DMD and averaged DMD. The superiority of averaged DMD in preserving signal fidelity under varying SNR conditions underscores its robust denoising capabilities. Hence, the presented results not only validate the enhanced denoising proficiency of averaged DMD over the conventional DMD but also contribute nuanced insights into the differential impact of varying SNR levels on the performance of these modalities across distinct frequency components. Herein, the mutual coupling is modeled using a Toeplitz matrix, which is a common approach in ULA processing for its simplicity [50]. However, we acknowledge that this might not fully capture the complex coupling effects that can occur in practical scenarios. To address this, we could explore the use of unknown mutual coupling elements, which provide a more flexible, albeit complex, model that adapts to the actual data. In addition, using full-wave simulation could offer the most accurate results, accounting for the detailed electromagnetic interactions. The coupling-informed scheme could be designed and modified based on these different mutual coupling models in the future.

C. Estimation With Unknown Number of Sources

In the subsequent analysis, we address scenarios where the number of sources is not predetermined. Using the same simulation setup depicted in Fig. 3, initially designed for a known source number of 2, we extend our investigation. The DMD eigenvalues' distribution under the assumption of a known source number is portrayed in Fig. 4. We vary the truncation orders, specifically, 3, 4, 5, and 6, all of which exceed the actual source number. The resulting DMD spectrum

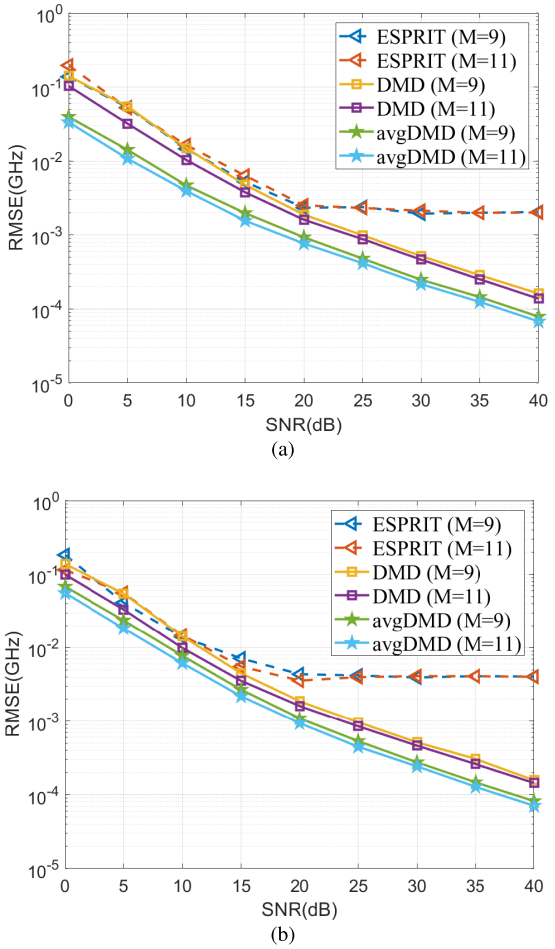

Fig. 10. Comparison of performance of frequency estimations for (a) source 1 and (b) source 2 obtained by the ESPRITR and proposed method at different SNRs with $M = 9$ and $M = 11$ in ULA.

is illustrated in Fig. 9. Notably, only eigenvalues with a real part equal to zero correspond to the authentic source signal, enabling the identification of two distinctive modes.

As shown in Fig. 4, it becomes evident that the proposed method facilitates accurate DOA information extraction even when the source number is unknown. This underscores the versatility of the proposed coupled-informed data-driven method for both known and unknown source number scenarios, establishing its utility in frequency and DOA estimation analyses.

D. Performance Analysis and Computational Complexity

For further validation, we executed a comparative analysis on the efficacy of frequency estimation for two distinct sources, as exhibited in Fig. 3(b), using a variety of estimation methodologies across an array of SNRs. Specifically, Fig. 10(a) and (b) presents the performance metrics for source 1 and source 2, respectively. The data are depicted as the root mean square error (RMSE) in gigahertz (GHz) plotted on a logarithmic scale versus the SNR in decibels (dB) on a linear scale. The comparative assessment includes the estimation of signal parameters via rotational invariance techniques (ESPRITs) and DMD, alongside the proposed avgDMD method, evaluated at two distinct parameter settings

(M = 9 and M = 11), representing the number of sensors within a ULA.

Distinct markers and colors within the plots denote each method, with the plots demonstrating a downward trend, indicating that an increase in SNR correlates with a reduction in RMSE across all the methods. This trend aligns with the theoretical prediction that superior SNR levels should result in enhanced frequency estimation accuracy. Furthermore, a higher count of antennas, represented by the parameter settings, is shown to reduce RMSE for each method. Crucially, the avgDMD method consistently achieved the lowest RMSE across the spectrum of SNRs tested, suggesting that the proposed avgDMD method surpasses the other methods in comparison. Consequently, we infer that the proposed avgDMD method exhibits robust performance and is suitably equipped for application in noisy operational environments. Notably, when the mutual coupling effects are consistent across sources, our method effectively handles the spatial distribution, as demonstrated by incorporating a Toeplitz matrix into the spatial signal decomposition. However, when mutual coupling effects vary between sources, the array manifold changes, complicating the decomposition process. This variability in the array response matrix poses challenges in effectively integrating the mutual coupling matrix. In cases where the coupling matrix is entirely random, the signal estimation problem may become underdetermined, raising concerns about the convergence of our method.

V. Conclusion

In conclusion, we develop a novel coupling-informed data-driven approach, Schur-averaged DMD, for concurrent DOA and frequency estimation in a ULA under the influence of mutual coupling and high noise levels. The significance of our contribution lies in seamlessly integrating coupling information into the data-driven framework, enhancing the accuracy and robustness of joint DOA and frequency estimation in realistic scenarios. The incorporation of moving averaging technology within the DMD framework fortifies anti-noise capabilities, ensuring a more accurate decomposition of signal components in the presence of noise. The inherent one-to-one correspondence between eigenvalues and eigenvectors streamlines the joint estimation process, automating the pairing of frequency and DOA without additional matching steps. Notably, our method exhibits adaptability to scenarios with an unknown number of sources, determined through the analysis of eigenvalue distribution. This feature enhances the practical applicability of our approach in real-world scenarios where source numbers may be previously unknown. Hence, our work advances the state-of-the-art in DOA and frequency estimation, offering a versatile and robust solution for complex scenarios.

Appendix
Implementation of DMD

The SVD is first computed for $\mathbf{X}_1$ which can be written as

$$\mathbf{X}_1 = \mathbf{U}\boldsymbol{\Sigma}\mathbf{V}^* \tag{27}$$

where $*$ means the conjugate transpose. Substituting (27) into (11) and through simple calculation, the mapping matrix can be derived as

$$\mathbf{B} = \mathbf{X}_2\mathbf{V}\boldsymbol{\Sigma}^{-1}\mathbf{U}^*. \tag{28}$$

Then, based on the following transform: $\tilde{\mathbf{X}}_1 = \mathbf{U}^*\mathbf{X}_1$, $\tilde{\mathbf{X}}_2 = \mathbf{U}^*\mathbf{X}_2$, and $\tilde{\mathbf{B}} = \mathbf{U}^*\mathbf{B}\mathbf{U}$, the efficient low-rank mapping relationships is obtained as $\tilde{\mathbf{X}}_2 = \tilde{\mathbf{B}}\tilde{\mathbf{X}}_1$. The eigendecomposition of $\tilde{\mathbf{B}}$ can capture the actual dynamics, which is obtained as

$$\tilde{\mathbf{B}}\mathbf{F} = \mathbf{F}\boldsymbol{\Lambda} \tag{29}$$

where $\mathbf{F}$ denotes a square matrix of order I, in which the columns refer to the eigenvectors. $\boldsymbol{\Lambda}$ refers to an diagonal matrix containing the corresponding eigenvalues $\lambda_i, i = 1, 2, \ldots, I$. Notably, considering there are only I actual incoming ray, the order I could be set to be the same as the number of actual incoming ray and then determined by truncated SVD in (27). Next, the dynamic modes in the original signal model in ULA are defined as

$$\mathbf{H} = \mathbf{X}_2\mathbf{V}\boldsymbol{\Sigma}^{-1}\mathbf{E}. \tag{30}$$

References

[1] B. Liao, A. Madanayake, and P. Agathoklis, "Array signal processing and systems," *Multidimensional Syst. Signal Process.*, vol. 29, no. 2, pp. 467–473, Apr. 2018.

[2] Z.-M. Liu, C. Zhang, and S. Y. Philip, "Direction-of-arrival estimation based on deep neural networks with robustness to array imperfections," *IEEE Trans. Antennas Propag.*, vol. 66, no. 12, pp. 7315–7327, Dec. 2018.

[3] S. Vigneshwaran, N. Sundararajan, and P. Saratchandran, "Direction of arrival (DoA) estimation under array sensor failures using a minimal resource allocation neural network," *IEEE Trans. Antennas Propag.*, vol. 55, no. 2, pp. 334–343, Feb. 2007.

[4] A. B. Baral and M. Torlak, "Joint Doppler frequency and direction of arrival estimation for TDM MIMO automotive radars," *IEEE J. Sel. Topics Signal Process.*, vol. 15, no. 4, pp. 980–995, Jun. 2021.

[5] J. Fuchs, M. Gardill, M. Lübke, A. Dubey, and F. Lurz, "A machine learning perspective on automotive radar direction of arrival estimation," *IEEE Access*, vol. 10, pp. 6775–6797, 2022.

[6] H. Lee, J. Ahn, Y. Kim, and J. Chung, "Direction-of-arrival estimation of far-field sources under near-field interferences in passive sonar array," *IEEE Access*, vol. 9, pp. 28413–28420, 2021.

[7] X. Pan, Z. Zhang, Y. Li, and W. Xu, "Fast estimation of direction of arrival based on sparse Bayesian learning for towed array sonar during manoeuvring," *IET Radar, Sonar Navigat.*, vol. 17, no. 7, pp. 1079–1087, Jul. 2023.

[8] B. Jalal, X. Yang, X. Wu, T. Long, and T. K. Sarkar, "Efficient direction-of-arrival estimation method based on variable-step-size LMS algorithm," *IEEE Antennas Wireless Propag. Lett.*, vol. 18, no. 8, pp. 1576–1580, Aug. 2019.

[9] H.-T. Chou, T.-W. Hsiao, and J.-H. Chou, "Active phased array of cavity-backed slot antennas with modified feeding structure for the applications of direction-of-arrival estimation," *IEEE Trans. Antennas Propag.*, vol. 66, no. 5, pp. 2667–2672, May 2018.

[10] K. Zhang et al., "Direction of arrival estimation and robust adaptive beamforming with unfolded augmented coprime array," *IEEE Access*, vol. 8, pp. 22314–22323, 2020.

[11] S. Jiang, N. Fu, Z. Wei, X. Li, L. Qiao, and X. Peng, "Joint spectrum, carrier, and DOA estimation with beamforming MWC sampling system," *IEEE Trans. Instrum. Meas.*, vol. 71, pp. 1–15, 2022.

[12] F. Wen, J. Wang, J. Shi, and G. Gui, "Auxiliary vehicle positioning based on robust DOA estimation with unknown mutual coupling," *IEEE Internet Things J.*, vol. 7, no. 6, pp. 5521–5532, Jun. 2020.

[13] J. Li, Y. Wang, Z. Ren, X. Gu, M. Yin, and Z. Wu, "DOA and range estimation using a uniform linear antenna array without *a priori* knowledge of the source number," *IEEE Trans. Antennas Propag.*, vol. 69, no. 5, pp. 2929–2939, May 2021.

[14] F. Wang, Z. Tian, G. Leus, and J. Fang, "Direction of arrival estimation of wideband sources using sparse linear arrays," *IEEE Trans. Signal Process.*, vol. 69, pp. 4444–4457, 2021.

[15] H. Wang, L. Wan, M. Dong, K. Ota, and X. Wang, "Assistant vehicle localization based on three collaborative base stations via SBL-based robust DOA estimation," *IEEE Internet Things J.*, vol. 6, no. 3, pp. 5766–5777, Jun. 2019.

[16] E. Gentilho, P. R. Scalassara, and T. Abrão, "Direction-of-arrival estimation methods: A performance-complexity tradeoff perspective," *J. Signal Process. Syst.*, vol. 92, no. 2, pp. 239–256, Feb. 2020.

[17] N. Ahmed et al., "Performance analysis of efficient computing techniques for direction of arrival estimation of underwater multi targets," *IEEE Access*, vol. 9, pp. 33284–33298, 2021.

[18] B. Liao, Z.-G. Zhang, and S.-C. Chan, "DOA estimation and tracking of ULAs with mutual coupling," *IEEE Trans. Aerosp. Electron. Syst.*, vol. 48, no. 1, pp. 891–905, Jan. 2012.

[19] Z. Ye and C. Liu, "2-D DOA estimation in the presence of mutual coupling," *IEEE Trans. Antennas Propag.*, vol. 56, no. 10, pp. 3150–3158, Oct. 2008.

[20] J. Dai, X. Bao, N. Hu, C. Chang, and W. Xu, "A recursive RARE algorithm for DOA estimation with unknown mutual coupling," *IEEE Antennas Wireless Propag. Lett.*, vol. 13, pp. 1593–1596, 2014.

[21] Y. Yu, H.-S. Lui, C. H. Niow, and H. T. Hui, "Improved DOA estimations using the receiving mutual impedances for mutual coupling compensation: An experimental study," *IEEE Trans. Wireless Commun.*, vol. 10, no. 7, pp. 2228–2233, Jul. 2011.

[22] K. M. Pasala and E. M. Friel, "Mutual coupling effects and their reduction in wideband direction of arrival estimation," *IEEE Trans. Aerosp. Electron. Syst.*, vol. 30, no. 4, pp. 1116–1122, Apr. 1994.

[23] R. S. Adve and T. K. Sarkar, "Compensation for the effects of mutual coupling on direct data domain adaptive algorithms," *IEEE Trans. Antennas Propag.*, vol. 48, no. 1, pp. 86–94, Jan. 2000.

[24] Y. Wang, M. Trinkle, and B. Ng, "DOA estimation under unknown mutual coupling and multipath with improved effective array aperture," *Sensors*, vol. 15, no. 12, pp. 30856–30869, Dec. 2015.

[25] B. C. Ng and C. M. S. See, "Sensor-array calibration using a maximum-likelihood approach," *IEEE Trans. Antennas Propag.*, vol. 44, no. 6, pp. 827–835, Jun. 1996.

[26] F. Sellone and A. Serra, "A novel online mutual coupling compensation algorithm for uniform and linear arrays," *IEEE Trans. Signal Process.*, vol. 55, no. 2, pp. 560–573, Feb. 2007.

[27] O. J. Famoriji and T. Shongwe, "Electromagnetic machine learning for estimation and mitigation of mutual coupling in strongly coupled arrays," *ICT Exp.*, vol. 9, no. 1, pp. 8–15, Feb. 2023.

[28] J. Cong, X. Wang, M. Huang, and L. Wan, "Robust DOA estimation method for MIMO radar via deep neural networks," *IEEE Sensors J.*, vol. 21, no. 6, pp. 7498–7507, Mar. 2021.

[29] O. J. Famoriji, O. Y. Ogundepo, and X. Qi, "An intelligent deep learning-based direction-of-arrival estimation scheme using spherical antenna array with unknown mutual coupling," *IEEE Access*, vol. 8, pp. 179259–179271, 2020.

[30] W. Fang et al., "A lightweight deep learning-based algorithm for array imperfection correction and DOA estimation," *J. Commun. Inf. Netw.*, vol. 7, no. 3, pp. 296–308, Sep. 2022.

[31] W. Fang et al., "A deep learning based mutual coupling correction and DOA estimation algorithm," in *Proc. 13th Int. Conf. Wireless Commun. Signal Process. (WCSP)*, Oct. 2021, pp. 1–5.

[32] C. H. Niow and H. T. Hui, "Improved noise modeling with mutual coupling in receiving antenna arrays for direction-of-arrival estimation," *IEEE Trans. Wireless Commun.*, vol. 11, no. 4, pp. 1616–1621, Apr. 2012.

[33] Y. Wang, X. Yang, J. Xie, L. Wang, and B. W.-H. Ng, "Sparsity-inducing DOA estimation of coherent signals under the coexistence of mutual coupling and nonuniform noise," *IEEE Access*, vol. 7, pp. 40271–40278, 2019.

[34] J.-D. Lin, W.-H. Fang, Y.-Y. Wang, and J.-T. Chen, "FSF MUSIC for joint DOA and frequency estimation and its performance analysis," *IEEE Trans. Signal Process.*, vol. 54, no. 12, pp. 4529–4542, Dec. 2006.

[35] L. Liu, J.-F. Gu, and P. Wei, "Joint DOA and frequency estimation with sub-Nyquist sampling," *Signal Process.*, vol. 154, pp. 87–96, Jan. 2019.

[36] M. Wax and T. Kailath, "Detection of signals by information theoretic criteria," *IEEE Trans. Acoust., Speech, Signal Process.*, vol. ASSP-33, no. 2, pp. 387–392, Apr. 1985.

[37] M. Wang, Q. Shen, W. Liu, and W. Cui, "Wideband DOA estimation with frequency decomposition via a unified GS-WSpSF framework," *IEEE Trans. Aerosp. Electron. Syst.*, vol. 60, no. 2, pp. 2453–2460, Apr. 2024.

[38] Y. Fang, S. Zhu, Y. Gao, L. Lan, C. Zeng, and Z. Liu, "Direction-of-arrival estimation of coherent signals for uniform linear antenna arrays with mutual coupling in unknown nonuniform noise," *IEEE Trans. Veh. Technol.*, vol. 71, no. 2, pp. 1656–1668, Feb. 2022.

[39] Y. Wang, L. Wang, J. Xie, M. Trinkle, and B. W.-H. Ng, "DOA estimation under mutual coupling of uniform linear arrays using sparse reconstruction," *IEEE Wireless Commun. Lett.*, vol. 8, no. 4, pp. 1004–1007, Aug. 2019.

[40] Z. Ye and C. Liu, "Non-sensitive adaptive beamforming against mutual coupling," *IET Signal Process.*, vol. 3, no. 1, p. 1, 2009.

[41] B. Liao and S.-C. Chan, "Adaptive beamforming for uniform linear arrays with unknown mutual coupling," *IEEE Antennas Wireless Propag. Lett.*, vol. 11, pp. 464–467, 2012.

[42] Y. Zhang and L. Jiang, "A novel data-driven scheme for the ship wake identification on the 2-D dynamic sea surface," *IEEE Access*, vol. 8, pp. 69593–69600, 2020.

[43] P. J. Schmid, "Dynamic mode decomposition of numerical and experimental data," *J. Fluid Mech.*, vol. 656, pp. 5–28, Jul. 2010.

[44] Y. Zhang and L. Jiang, "A novel demultiplexing scheme for vortex beams in radio communication systems," *IEEE Trans. Veh. Technol.*, vol. 70, no. 7, pp. 7243–7248, Jul. 2021.

[45] Y. Zhang, M. L. N. Chen, and L. J. Jiang, "Analysis of electromagnetic vortex beams using modified dynamic mode decomposition in spatial angular domain," *Opt. Exp.*, vol. 27, no. 20, p. 27702, 2019.

[46] Y. Zhang, L. Jiang, and H. T. Ewe, "A novel data-driven modeling method for the spatial–temporal correlated complex sea clutter," *IEEE Trans. Geosci. Remote Sens.*, vol. 60, 2022, Art. no. 5104211.

[47] Y. Zhang and L. Jiang, "A novel data-driven analysis method for electromagnetic radiations based on dynamic mode decomposition," *IEEE Trans. Electromagn. Compat.*, vol. 62, no. 4, pp. 1443–1450, Aug. 2020.

[48] H. Park and L. Eldén, "Schur-type methods for solving least squares problems with Toeplitz structure," *SIAM J. Sci. Comput.*, vol. 22, no. 2, pp. 406–430, Jan. 2000.

[49] X.-G. Lv and T.-Z. Huang, "The inverses of block Toeplitz matrices," *J. Math.*, vol. 2013, Aug. 2013, Art. no. 207176.

[50] B. Friedlander, "On the mutual coupling matrix in array signal processing," in *Proc. 54th Asilomar Conf. Signals, Syst., Comput.*, Nov. 2020, pp. 1245–1249.

Yanming Zhang (Member, IEEE) received the B.Eng. degree in electrical engineering from China University of Mining and Technology, Xuzhou, China, in 2015, the M.S. degree in information engineering from Southeast University, Nanjing, China, in 2018, and the Ph.D. degree in electrical and electronic engineering from the University of Hong Kong, Hong Kong, in 2022.

From February 2022 to September 2022, he was a Post-Doctoral Fellow with the Department of Electrical and Electronic Engineering, The University of Hong Kong. Since October 2022, he has been a Post-Doctoral Fellow with the Department of Electronic Engineering, The Chinese University of Hong Kong, Hong Kong. His current research interests include computational electromagnetics and data-driven methods.

Wenchao Xu (Member, IEEE) received the B.E. and M.E. degrees from Zhejiang University, Hangzhou, China, in 2008 and 2011, respectively, and the Ph.D. degree from the Department of Electrical and Computer Engineering, University of Waterloo, Waterloo, Canada, in 2018.

He is currently a Research Assistant Professor with the Hong Kong Polytechnic University. In 2011, he joined Alcatel Lucent Shanghai Bell Company Ltd., where he was a Software Engineer for telecom virtualization. He has published over 100 research papers at top-tier journals including Proceedings of IEEE, IEEE TRANSACTIONS ON PARALLEL AND DISTRIBUTED SYSTEMS, IEEE TRANSACTIONS ON MOBILE COMPUTING, and prestigious conferences including IEEE/CVF CVPR, ICML, NeurIPS, IEEE INFOCOM, and IEEE ICDCS. His research areas include mobile computing, AI enabled networking, multimodal learning, and the Internet of vehicles.

A-Long Jin (Member, IEEE) received the B.Eng. degree in communications engineering from Nanjing University of Posts and Telecommunications, Nanjing, China, in 2012, the M.Sc. degree in computer science from the University of New Brunswick, Canada, in 2015, and the Ph.D. degree in electrical and electronic engineering from the University of Hong Kong, Hong Kong, in 2023.

He is currently an Assistant Professor at Xi'an Jiaotong-Liverpool University. His research interests include computer networks and distributed systems.

Min Li (Member, IEEE) received the B.S. degree from the University of Electronic Science and Technology of China, Chengdu, China, in 2014, and the Ph.D. degree from The University of Hong Kong (HKU), Hong Kong, in 2018.

He currently holds the position of Professor at Tianjin University (TJU). Before joining TJU in 2024, he held several positions including Post-Doctoral Researcher at HKU from 2018 to 2021, Research Assistant Professor at The Hong Kong University of Science and Technology (HKUST), from 2021 to 2022, Post-Doctoral Researcher at the University of California, Los Angeles (UCLA), from 2022 to 2023, and Assistant Professor at Heriot-Watt University, U.K., from 2023to 2024. His research interests encompass microwaves, antennas, applied electromagnetics, and MIMO communications.

Peifeng Ma (Senior Member, IEEE) received the M.S. degree in signal and information processing from the Institute of Remote Sensing and Digital Earth, Chinese Academy of Sciences, Beijing, China, in 2012, and the Ph.D. degree in earth system and geo information science from the Institute of Space and Earth Information Science, The Chinese University of Hong Kong, Shatin, Hong Kong, in 2016.

He is currently an Assistant Professor at the Department of Geography and Resource Management, Institute of Space and Earth Information Science, The Chinese University of Hong Kong. He has published more than 50 research articles in high-impact peer-reviewed journals, such as Remote Sensing of Environment, IEEE TRANSACTIONS ON GEOSCIENCE AND REMOTE SENSING, and *ISPRS Journal of Photogrammetry and Remote Sensing*. He is the Principal Coordinator of the project "Development of an intelligent infrastructural health diagnosis-oriented SAR Interferometry (InSAR) platform" in Hong Kong. His research interests include persistent scatterer interferometry, synthetic aperture radar (SAR) tomography, distributed scatterer interferometry, and their applications for urban infrastructural health monitoring and geo-hazard monitoring.

Lijun Jiang (Fellow, IEEE) received the bachelor's degree in electrical engineering from Beijing University of Aeronautics and Astronautics, Beijing, China, in 1993, the master's degree from the Tsinghua University, Beijing, in 1996, and the Ph.D. degree from the University of Illinois at Urbana-Champaign (UIUC), Champaign, IL, USA, in 2004.

From 1996 to 1999, he was an Application Engineer with Hewlett Packard Company. From 2004 to 2009, he was a Postdoc, Research Staff Member, and Senior Engineer with IBM T.J. Watson Research Center. He was an Associate Professor in December 2009, then the Honorable Associate Professor with the Department of Electrical and Electronics Engineering, The University of Hong Kong, where he received tenure in July 2014. From June 2013 to 2014, he was a Senior Visiting Professor with Tsinghua University. He was an occasional Visiting Scholar to Professor T. Itoh's Group with the University of California, Los Angeles, Los Angeles, CA, USA, from 2014 to 2018, where he spent his Sabbatical from September 2014 to March 2015. From September 2022 to August 2023, he joined the Department of Electrical Engineering, The Chinese University of Hong Kong as a Professor and an Associate Director of Center for Intelligent Electromagnetic Systems. Since September 2023, he has been a Kummer Endowed Professor with the Department of Electrical and Computer Engineering, Missouri University of Science and Technology, Rolla, MO, USA. His multidisciplinary research activities have resulted in leading research outputs around 170 peer-reviewed journal publications, many international and regional awards, multiple patents, and book/book chapters. His research interests include heterogeneous electromagnetic modeling methodologies, high speed electronic physical design and EDA solutions, SI/PI and EMC/EMI, antenna and microwave technologies, microwave engineering for linear and nonlinear artificial materials, nano structures, THz, and optics.

Dr. Jiang has been an ACES Fellow. He was the recipient of IEEE Technical Achievement Award, IBM Research Technical Achievement Award, UIUC Y.T.Lo Outstanding Research Award, and HP STAR Award. He is the Chair of IEEE APEMC International Steering Committee and Chair of IEEE (HK) EMC Chapter. He has served many top international conferences in his area as TPC Chairs, Session Chairs, Organization Committee Members, or Session Chairs. He was an Associate Editor or Guest Associate Editor for IEEE TRANSACTIONS ON ANTENNAS AND PROPAGATION, PROCEEDING OF IEEE, and IEEE TRANSACTIONS ON MICROWAVE THEORY AND TECHNIQUES. From 2020 to 2022, he was a member of IEEE AP Society Award Selection Committee.

Steven Gao (Fellow, IEEE) received the Ph.D. degree from Shanghai University, Shanghai, China.

He is a Professor at the Department of Electronic Engineering, The Chinese University of Hong Kong (CUHK), where he is also the Director of Centre for Intelligent Electromagnetic Systems, CUHK. He is an Honorary Professor at the University of Kent, U.K. Prior to joining CUHK, he worked at the UK universities for about 22 years and was a Professor and Chair of RF/Microwave Engineering at the University of Kent, U.K., during 2013 to 2022. He co-authored/co-edited three books (Space Antenna Handbook, Wiley, 2012; Circularly Polarized Antennas, IEEE & Wiley, 2014; Low-Cost Smart Antennas, Wiley, 2019), over 500 papers and 20 patents. His research covers smart antennas, phased arrays, MIMO, reconfigurable antennas, broadband/multiband antennas, satellite antennas, RF/microwave/mm wave/THz circuits, and wireless systems (mobile and satellite communications, synthetic aperture radars, IOT).

Dr. Gao is the Editor-in-Chief for IEEE ANTENNAS AND WIRELESS PROPAGATION LETTERS. He was a Distinguished Lecturer of IEEE Antennas and Propagation Society from 2014 to 2016, and an Associate Editor for several international Journals (IEEE TAP; *Radio Science*; *Electronics Letters*; *IET Circuits, Devices and Systems*). He served as the Lead Guest Editor of Proceedings of the IEEE for a Special Issue on "Small Satellites" (2018), and the Lead Guest Editor of IEEE TRANSACTIONS ON ANTENNAS AND PROPAGATION for Special Issues on "Low-Cost Wide-Angle Beam-Scanning Antennas" in 2022 and "Antennas for Satellite Communication" in 2015, and a Guest Editor of *IET Circuits, Devices & Systems* for a Special Issue in "Photonic and RF Communications Systems" in 2014. He was the U.K.'s Representative in European Association on Antennas and Propagation (EurAAP) during 2021 to 2022, General Chair or General Co-Chair of international conferences (LAPC 2013, UCMMT 2021) and was an Invited/Keynote Speaker at many conferences. He is TPC Chair of ISAPE 2024.